Cysteine-Functionalized Chitosan Magnetic Nano-Based Particles for the Recovery of Uranium(VI): Uptake Kinetics and Sorption Isotherms

Ahmed A. Galhoum, Mohammad G. Mahfouz, Nabawia A. Gomaa, Sayed S. Abdel-Rehem, Asem A. Atia, Thierry Vincent, Eric Guibal

Cysteine-Functionalized Chitosan Magnetic Nano-Based Particles for the Recovery of Uranium(VI): Uptake Kinetics and Sorption Isotherms

Ahmed A. Galhoum,[1,2] Mohammad G. Mahfouz,[1] Nabawia A. Gomaa,[1] Sayed S. Abdel-Rehem,[3] Asem A. Atia,[4] Thierry Vincent,[2] and Eric Guibal[2]

[1]*Nuclear Materials Authority, El-Maadi, Cairo, Egypt*
[2]*Ecole des mines d'Alès, Centre des Matériaux des Mines d'Alès, Alès cedex, France*
[3]*Department of Chemistry, Faculty of Science, Ain Shams University, Egypt*
[4]*Department of Chemistry, Faculty of Science, Menoufia University, Shebin El-Kom, Egypt*

Magnetic-chitosan nanoparticles, functionalized with cysteine, were synthesized and characterized by element analysis, FT-IR, XRD, TEM, and vibrating sample magnetometry. The sorbent was tested for U(VI) recovery, considering:

a. pH effect,
b. sorption isotherms (fitted by Langmuir equation), and
c. uptake kinetics (modeled using the PSORE).

Maximum sorption capacity approached 100 mg U g^{-1}. The nanometric size of sorbent reduces the impact of resistance to intraparticle diffusion; this may explain the fast kinetics (equilibrium within 50 min). The reaction is exothermic, spontaneous. The metal could be desorbed using acidified urea solution and the sorbent could be recycled for 5 cycles.

Keywords Cysteine-functionalized chitosan; uranium(VI); magnetic chitosan nano-based particles; sorption isotherm; uptake kinetics

INTRODUCTION

The most common isotope of natural uranium is ^{238}U, which has a negligible radiotoxicity, due to its geologically long half-life (4.5×10^9 years). However, because of its superior binding affinity toward biomolecules (1), ingestion and inhalation of uranium could cause certain acute and/or chronic harmful effects, especially in terms of kidney damage after drastic and/or long-term exposure to uranium-based compounds (1, 2). This is a highly bio-toxic metal while being introduced into fragile ecosystem through the combination of natural processes and anthropogenic activities (3). On the other hand, due to limited quantities of uranium minerals in nature and the intense use for energy production, shortage of uranium is expected in a few decades (4) and this makes the recovery of uranium from low-metal concentration effluents a strategic issue for the future of nuclear power industry. Recovery of uranium from dilute aqueous streams may be considered a complementary resource in addition to mining or recycling of end-of-life industrial materials (5). These processes may concern both industrial aqueous waste streams but also acid mine drainage from metal or coal mines (6), even from seawater (7). Therefore, separation and recovery of uranium from aqueous solutions are of great practical significance, not only in terms of reutilization of uranium resources and sustainable development of nuclear energy, but also for the protection of both human health and ecological environment (8).

Metals, such as uranium, may be recovered through different processes such as solvent extraction, ion-exchange or chelating resins (7), precipitation (5). The competitiveness of the process, its technical efficiency, and environmental effectiveness depend on the range of metal concentration, the complexity/composition of the solution, etc. Precipitation processes may produce a huge amount of contaminated sludge requiring appropriate storing conditions; solvent extraction is only competitive for concentrated solutions; conventional resins may be very expensive (9), and alternative sorbents such as biosorbents have been suggested for replacing these conventional methods (10, 11). A great diversity of materials of biological origin have been investigated for uranium recovery from dilute solutions; including fungal biomass (12), algal biomass (13), agriculture by-products (14, 15), or biopolymers issued from marine resources such as alginate (16) and chitosan (17, 18).

Chitosan, which is commercially produced from crustacean shells, is very reactive for metal sorption through different mechanisms such as:

Address correspondence to Eric Guibal or Ahmed A. Galhoum, Ecole des mines d'Alès, Centre des Matériaux des Mines d'Alès, C2MA/MPA/BCI, 6 avenue de Clavières, Alès cedex, France. E-mail : Eric.Guibal@mines-ales.fr or Galhoum_nma@yahoo.com

a. chelation of metal cations on free amine groups in near neutral solutions, and
b. ion-exchange for metal anions on protonated amine groups in acidic solutions (19).

In addition, chitosan can be used as a raw material for the design of chelating and ion-exchange resins by chemical derivatization (grafting of supplementary or complementary reactive groups) for improving the density of sorption sites, the selectivity of reactive groups, changing the sorption mechanisms, or extending the operative pH (19). The density of hydroxyl groups on chitosan backbone may explain its high hydrophilic behavior (especially compared with synthetic base materials, like polystyrene-divinylbenzene, polyethylene, and polyurethane); this may enhance sorption kinetic of ionic species in aquatic media (20, 21). Chelating or coordinating resins are polymers with covalently bound functional groups containing one or more donor atoms, which are capable of forming complexes directly with metal ions. These polymers can also be used for the specific separation of one or more metal ions from complex solutions (22). In chelating resins, the functional group atoms the most frequently used are nitrogen (e.g., N in amines, azo groups, amides, nitriles), oxygen (e.g., O in carboxylic, hydroxyl, phenolic, ether, carbonyl, phosphoryl groups) and sulfur (e.g., S in thiols, thiocarbamates, thio-ethers). The anchored molecules may contribute to the selective extraction of metal cations (23). Several chelating ligands such as catechol, iminodiacetic acid, iminodimetyl-phosphonic acid, phenylarsonic acid, or serine (24) and amino acids moieties (glycine, valine, leucine, and serine) (25) were used to functionalize crosslinked chitosan for sorption of uranium(VI) metal ions.

One of the major drawbacks of chitosan-based materials is associated with the poor porosity (and low specific surface area) of the biopolymer that imparts significant resistance to intraparticle diffusion. This effect can be minimized using:

a. conditioned materials (preparing chitosan gel beads, membranes, fibers, hollow fibers, and sponges) (26), or
b. decreasing the size of sorbent particles.

The micro- or nano-sizing of sorbent particles may cause serious problems for managing fixed-bed column systems (with clogging, head loss of pressure) or batch system (material recovery and handling at the end of the process). Nanomaterials have received great attention in other emerging and rapidly growing fields making profit of their good performance due to high specific surface area and limited resistance to intraparticle diffusion (20). The difficulty in recovering the nanoparticles by filtration or centrifugation may explain the limited development of these processes at large scale. This problem may be overcome using magnetic nano-based particles that can be readily handled and recovered using external magnetic field. Magnetic particles are usually composed of a magnetic core (to ensure a strong magnetic response) and a polymeric shell to hold favorable functional groups and feature sorption applications (27).

This work focuses on:

a. the synthesis of magnetic nano-based particles of chitosan functionalized with cysteine,
b. the characterization of the sorbent with FT-IR, XRD, TEM and VSM (vibrating sample magnetometer) analyses, and
c. the study of U(VI) sorption properties in slightly acidic solutions.

MATERIAL AND METHODS

Materials and Analytical Procedures

Chitosan (90.5% deacetylation degree) and diethylenetriamine (98%) were supplied by Sigma-Aldrich (France). Epichlorohydrin (> 98%), 1,4-dioxane (99.9%), ethanol, and arsenazo III (A.R. grade) were purchased from Fluka Chemika AG (Switzerland). All other chemicals were Prolabo (France) products and were used as received. Uranium stock solution was prepared from $UO_2(OCOCH_3)_2{\cdot}2H_2O$ supplied by Sigma-Aldrich in concentrated sulfuric acid under heating and diluted with distilled water until final concentration of 1000 g L^{-1}. The working solutions were prepared by appropriate dilution of the stock solution immediately prior to use. Uranium concentrations in solution were determined by spectrophotometry (Arsenazo III colorimetric method) (28) using a "Metertech Inc" model SP-8001 (UV–Visible spectrophotometer).

Sorbent Synthesis

Preparation of Cross-Linked Chitosan–Magnetic Nano-Based Particles

Chitosan–magnetic nano-based particles were prepared by chemical co-precipitation of Fe(II) and Fe(III) ions using NaOH for pH control in the presence of chitosan, followed by hydrothermal treatment (29). Chitosan (4 g) was dissolved in 200 mL (20% w/w) acetic acid solution; $FeSO_4$ and $FeCl_3$ (1:2 molar ratio: 6.62 g $FeSO_4.7H_2O$ and 8.68 g $FeCl_3$, respectively) were dissolved in the biopolymer solution. The resulting solution was chemically precipitated at 40°C by addition of NaOH (2 M) dropwise with constant stirring: the pH was controlled to 10–10.4. The suspension was heated at 90°C for 1 h under continuous stirring and finally separated by decantation. Then a solution of 0.01 M epichlorohydrin (containing 0.067 M sodium hydroxide) was prepared (pH close to 10) and added to the freshly prepared wet magnetic-chitosan particles (weight ratio of 1:1). The mixture of chitosan-magnetic particles and epichlorohydrin was heated at 40-50°C for 2 h under continuous stirring (30). The products were filtered and washed intensively with demineralized water to remove any unreacted epichlorohydrin.

Preparation of Cysteine-Functionalized Chitosan–Magnetic Nano-Based Particles

The amino acid moiety (cysteine) was grafted to crosslinked magnetic chitosan particles in two steps (25): First, the crosslinked chitosan (ii) was suspended in 150 mL ethanol/water mixture (1:1 v/v); then, epichlorohydrin (15 mL) was added to the suspension, and the mixture was refluxed for 4 h. After the reaction, the product (iii) was filtered and washed 3 times with ethanol and with ultrapure water to remove any residual reagents. Secondly, the washed product (iii) and cysteine (16 g) were suspended in dioxane (200 mL). The mixture was alkalinized to pH 9.5-10 using 1 M NaOH solution; the mixture was refluxed for 6 h. After the reaction, the final product was filtered and washed 3 times with ethanol and with ultrapure water. Finally, the product was freeze-dried.

The amine content in the sorbent was estimated using a volumetric method as follows (31): 30 mL of 0.05 M HCl solution was added to 0.1 g of sorbent and conditioned for 15 h on a reciprocal shaker. The residual concentration of HCl was estimated through titration against 0.05 M NaOH solution using phenolphthalein as the indicator. The number of moles of HCl that interacted with amino group, and consequently the concentration of amino group in the sorbent (mmol g^{-1}) was calculated from Eq. (1):

$$\text{Concentration of amino group} = (M_1 - M_2) \times 30/0.1 \quad (1)$$

where M_1 and M_2 are the initial and final concentration of HCl, respectively.

Characterization Methods

The resin was chemically characterized by element analysis using an automatic analyzer CHNS Vario EL III-elementar analyzer (Elementar, Germany) for the determination of carbon, hydrogen, nitrogen, and sulfur elements in the final sorbent. Powder X-ray diffraction (XRD) patterns were obtained at room temperature using an X-ray diffraction unit (Philips model PW 3710/31, with generator PW1830 and scintillation counter PW 3020) using CuK_α radiation in the range of 2θ = 10–90°. The magnetic properties were measured on a vibrating sample magnetometer (VSM) (730T, Lakeshoper, America) at room temperature. The dimension and morphology of sorbent particles were observed by atomic force microscopy (AFM) (Shimadzu, Japan) and high resolution transmission electron microscope-HRTEM (JEOL-2100, Japan). Functional groups of adsorbent were analyzed with a Fourier Transform infrared spectroscopy FT-IR spectrometer Nicolet Nexus 870 FTIR spectrometer (Nicolet, USA). The scanning range was set between 4000 and 400 cm^{-1} and samples were conditioned using the KBr pellet technique.

Sorption and Desorption Experiments

Batch experiments were carried out by contact of a given mass of sorbent (i.e., m: 0.05 g) with a fixed volume of aqueous solution (i.e., V: 50 mL) containing a fixed concentration of uranium (i.e., C_0: 110 mg U L^{-1}) in a conical flask. The sorption experiments were agitated and performed at 200 rpm at room temperature (i.e., 25 ± 1°C) for 2 h. After equilibrium and phase separation (magnetic separation), the uranium concentration in the aqueous phase (C_{eq}, mg U L^{-1}) was determined by the Arsenazo III colorimetric method and the amount of uranium on the sorbent (q_e, mg U g^{-1}) was calculated by the mass balance equation:

$$q_e = (C_0 - C_{eq}) \text{x } V/M \quad (2)$$

The distribution coefficient K_d is obtained by the following equation:

$$K_d = [(C_0 - C_{eq})/C_{eq}] \text{x } V/M \quad (3)$$

All the measurements were duplicated and the experimental dispersion did not exceed 5%.

All experiments were carried out by equilibrating for 50 min at room temperature (25 ± 1°C) and pH 3.61 ± 0.01 with an initial concentration C_0: 110 mg U L^{-1}; except when the effect of time, pH, and metal concentration was studied. Detailed experimental conditions are reported in the caption of figures.

To evaluate the reusability of the sorbent, sorption of uranium(VI) and regeneration of U(VI)-loaded sorbent were performed along five successive sorption–desorption cycles with the same adsorbent. Fifty mg of sorbent were mixed with 50 mL of a 250 mg L^{-1} U(VI) solution in a conical flask and agitating in a shaker for 45 min at 25°C. The sorbent was separated magnetically; uranium concentration in the supernatant was estimated. The U(VI)-loaded sorbent, after gentle washing with demineralized water, was mixed with 50 mL of a 0.5 M solution of acidified urea in a shaker for 45 min, at 25 ± 1°C. After magnetic separation the sorbent was rinsed with demineralized water and re-used for sorption tests.

RESULTS AND DISCUSSION

Preparation of Magnetic Chitosan Nano-based Particles and Functionalized Material

A simple one-pot in situ co-precipitation method was used to synthesize magnetic chitosan nano-based particles. Chitosan precipitates in alkaline conditions simultaneously to the synthesis of magnetic iron particles (reaction between Fe(II) and Fe (III) under alkaline hydrothermal conditions) resulting in the formation of composite magnetite-chitosan particles. The dropwise addition of NaOH in the mixture controls the formation of nanometric-size of chitosan-magnetite particles (29). Chitosan-magnetite particles can be chemically modified to prevent their dissolution in acidic media; however, aldehyde-crosslinking

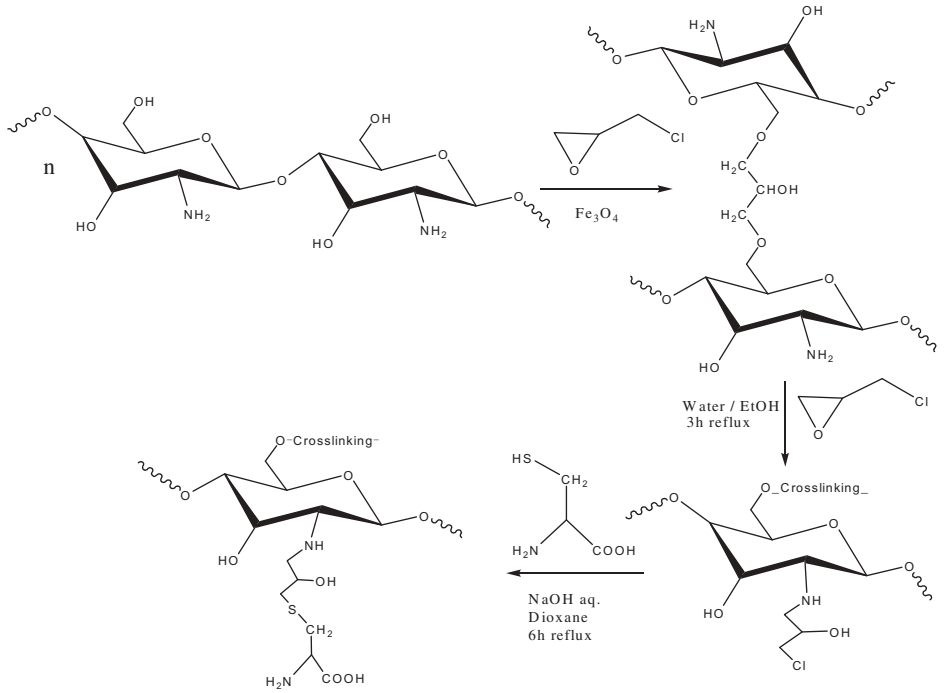

FIG. 1. Scheme for the synthesis of cysteine-functionalized chitosan magnetic nano-based particles.

may result in the loss of sorption capacity because some amine groups are involved in the crosslinking reaction (32, 33); so, epichlorohydrin (also called chloromethyloxirane) had been used as the crosslinking agent. Indeed, the crosslinking mono-functional agent is used to form covalent bonds with the carbon atoms linked to the hydroxyl groups of chitosan, resulting in the rupture of the epoxide ring and the removal of a chlorine atom (34). Figure 1 shows the synthesis route for cysteine functionalized magnetite-chitosan.

Characterization of Sorbents

Element Analysis

The C, H, N, and S contents in the crosslinked chitosan-magnetic nano-based particles were 14.23%, 2.55%, 1.71%, and 0%, respectively. After cysteine grafting, the C, H, N, and S contents increased to 19.84%, 3.93%, 3.14%, and 2.34%, respectively. The increases of carbon, hydrogen, nitrogen, and sulfur contents clearly show the successful grafting of cysteine moiety onto crosslinked chitosan magnetic nano-based particles (with spacer arm matrix).

FT-IR Spectrometry

FTIR spectra were recorded at each step of the synthesis to confirm the successive changes in the structure of the biopolymer (Fig. 2). Several typical bands can be detected. The band at 568 cm^{-1} is assigned to Fe-O stretching vibration of Fe_3O_4 (29, 33, 35). For the magnetic-chitosan composite (a) a strong and broad band appears around

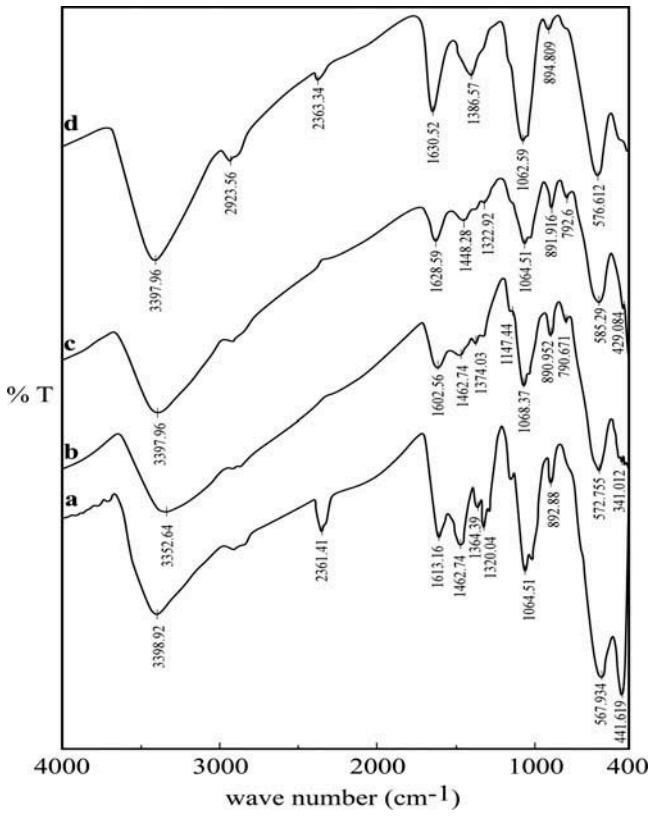

FIG. 2. FT-IR spectra of (a) chitosan-magnetite nanoparticles, (b) after crosslinking, (c) crosslinked chitosan magnetite with spacer arm and (d) cysteine-functionalized chitosan magnetic nano-based particles.

3399 cm^{-1}: this is generally attributed to the contributions of stretching vibration of –OH group, stretching vibration of N–H group and hydrogen bonds of polysaccharides. Another characteristic peak of primary amine $–NH_2$ appears at 1613 cm^{-1} (bending vibration). The bands at 1463 and 1364 cm^{-1} can be attributed to the C–O–C stretching or amide II and –OH bending vibrations, respectively. The absorption band at 893 cm^{-1} corresponds to β-D-glucose unit (18). The absorption bands around 1320 and 1065 cm^{-1} are generally assigned to the stretching vibrations of primary –OH group and secondary –OH group, respectively. After crosslinking (b), the absorption intensities of $–NH_2$ group and –OH obviously decrease compared with reference initial material (a): this confirms that the crosslinking reaction occurred with amino groups and –OH groups from vicinal polymer chains through epichlorohydrin (18).

The introduction of spacer arms on crosslinked chitosan is expected to involve the appearance of $–CH_2–Cl$ whose stretching vibration was assigned to a new band at 523 cm^{-1} (36) and this band is not clearly identified on the spectrum of the compound bearing epichlorohydrin spacer arms (c). Actually a new band (which could be assigned to the stretching vibration of –C-Cl, in the range 800-700 cm^{-1}, (37)) appears around 792 cm^{-1} after reaction with epichlorohydrin (cross-linking and grafting of spacer arms; i.e., on b and c spectra) but almost disappears after cysteine grafting (spectrum d). After grafting spacer arms (supplementary treatment with epichlorohydrin, spectrum c) and cysteine grafting (spectrum d) the 1613-1603 cm^{-1} band is shifted toward higher frequencies (1629-1631 cm^{-1}). This may be attributed to a change in the chemical environment of amine groups (including the formation of amide groups) and/or the grafting of carboxylic groups (from cysteine) (24, 37). In addition, the relative intensity of the band at 1387 cm^{-1} increases in the spectrum of cysteine-type material; this could be also attributed to either or both the grafting of amino groups and carboxylic acid moieties. The band around 1462 cm^{-1} (ascribed to amide II group (33)) is disappearing after cysteine grafting on chitosan; new free amine groups are added on the spacer arm of the sorbent. The values of amine group concentration of the cysteine adsorbent were found to be 3.53 mmol g^{-1}: this is about 24% more than in the spacer-arm-grafted crosslinked material.

X-ray Diffraction

X-ray diffraction pattern of cysteine-functionalized chitosan magnetic nano-based particles is shown in Fig. 3, together with the assignments of the different peaks, which are representative of Fe_3O_4: (111), (220), (311), (400), (422), (511), (440), and (622) (appearing at 2θ: 18.0, 30.1, 35.4, 43.0, 53.5, 57.0, 62.5, and 74.4, respectively). These peaks are consistent with the assignments reported in database JCPDS file (PDF No. 65-3107) (33, 35, 38). This confirms the presence of iron oxide particles (Fe_3O_4) with a spinel structure (usually associated with cubic close-packed oxides with one octahedral and two tetrahedral sites) which has magnetic properties; this makes the particles ready for magnetic separation. The half width at half maximum was used for calculating the particles size using the Debye-Scherrer equation (39):

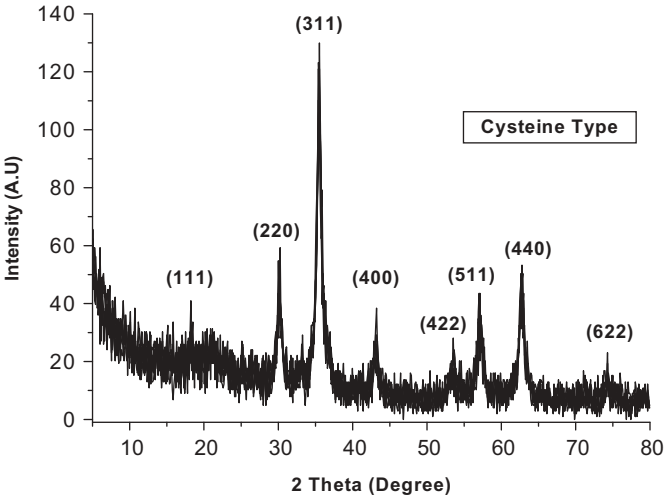

FIG. 3. Powder X-ray diffraction (XRD) patterns of cysteine-functionalized chitosan magnetic nano-based particles.

$$D = k\lambda / \beta \cos\theta \quad (4)$$

where D is the average diameter of nanoparticles, λ is the wavelength of X-ray radiation (1.5418 Å), θ is the diffraction angle, k = 0.9 (shape parameter) and β is the full width at half maximum of X-ray diffraction peaks. The crystal size has been found to be close to 13.5 nm using the (311) index.

Transmission Electron Microscopy

The TEM image of the sorbent (Fig. 4) shows that

a. particles have a spherical morphology, and
b. they are homogeneously distributed in size.

The structure of the adsorbents was monodisperse, characterized by a partial aggregation that led to an average diameter of 15–40 nm. This is probably due to the self-association of nanoparticles caused by the dipole-dipole attraction of magnetic cores. In addition, TEM photograph shows that the particles are “bi-color”;

a. dark central area corresponding to the magnetic core (crystalline Fe_3O_4), and
b. peripheral bright zone, which is associated with cysteine-functionalized chitosan.

These changes in color can be explained by the difference in electron-absorbing behavior of dense and heavy structure of

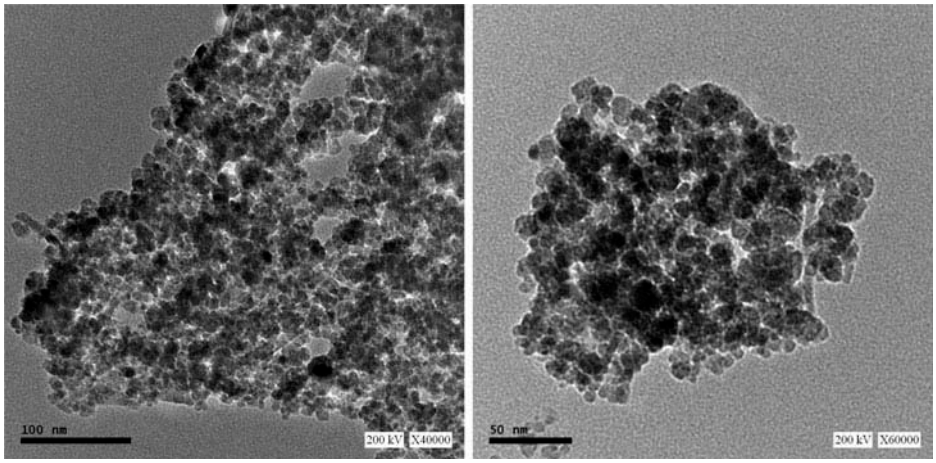

FIG. 4. TEM micrographs of cysteine-functionalized chitosan magnetic nano-based particles (the bars represent 50 and 100 nm, respectively).

mineral core and the light biopolymer coating. The coating of magnetic cores with chitosan appears to be thick and homogeneous.

Magnetic Properties: Vibrating Sample Magnetometry

Figure 5 shows the typical magnetization loop for cysteine-functionalized chitosan magnetic nano-based particles. There was no remanence and coercivity (no hysteresis loop). This means that chitosan–Fe_3O_4 nanoparticles are superparamagnetic. The saturation magnetization was calculated to be about 21.51 emu g^{-1} (21.51 A m^2 kg^{-1}). This value is significantly higher than the value (5.8 emu g^{-1}) reached with chitosan encapsulation of pre-formed magnetic nanoparticles (40). Therefore, the magnetic chitosan nanoparticles can be easily separated with the help of an external magnetic field. This may be very helpful for solid/phase separation or for handling the material in a hazardous environment.

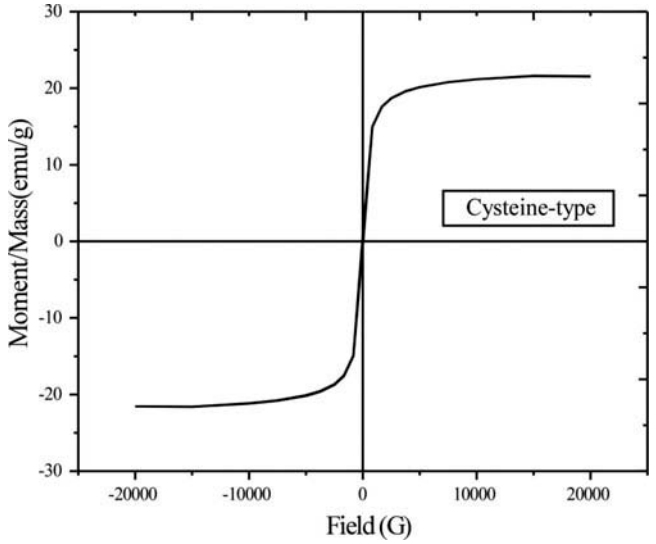

FIG. 5. Magnetization curves of cysteine-functionalized chitosan magnetic nano-based particles.

Sorption Properties

Effect of pH on Sorption Properties

The pH of the aqueous solution plays an important role in the whole sorption process and particularly on the sorption capacity, influencing the surface charge of the sorbent, the degree of ionization of the materials, through the dissociation of functional groups such as carboxyl, hydroxyl, and amino groups. It can also influence the aqueous chemistry of uranium (41). The influence of initial solution pH was investigated within the range 1-5-6.7, controlled using either 0.5 M H_2SO_4 or 0.5 M NaOH. At pH higher than 6.7, precipitation of uranyl ions as $UO_2(OH)_2$ may spontaneously occur (depending on metal concentration), making difficult the interpretation of sorption for high relative metal concentrations. On the opposite hand, the inorganic magnetic material may also dissolve at pH below 1.6.

Figure 6 shows the influence of initial pH on U(VI) sorption capacity using cysteine-functionalized chitosan magnetic nano-based particles. The figure also shows pH variation during metal uptake. The pH remains constant in the range 1.6-2.5, and then it significantly increases in the range 2.5-5 before tending to remain unchanged (pH_i: 5-6.7); for pH_i varying between 3.6 and 5.0, the equilibrium pH (pH_f) stabilized in the range 5.0-5.7. The sorption capacity progressively increases with pH in the range pH_i 1.6-3.6 (i.e., pH_f: 1.6-4.9) from 20 to 80 mg U g^{-1}. Above pH_i 3.6 (i.e., pH_f 5) the sorption capacity stabilizes around 80 mg U g^{-1}. Above pH_i 6.5 (i.e., pH_f 7), a new slight increase in sorption capacity is observed, probably associated with hydrolysis and precipitation effects. Above pH 6.5 uranyl ions form colloidal species that can

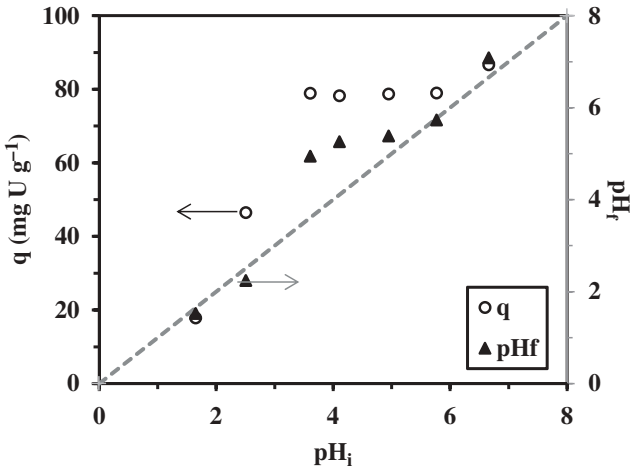

FIG. 6. Effect of pH on U(VI) sorption using cysteine-functionalized chitosan magnetic nano-based particles (C_O: 110 mg L^{-1}; T: 25 ± 1°C; time: 1 h; sorbent dosage, SD: 1 g L^{-1}; pH_i: initial pH; pH_f: equilibrium pH).

precipitate in the solution or at the surface of the sorbent making complex the interpretation of sorption performance.

The pH effect on U(VI) sorption may be explained by the contribution of different factors, and different mechanisms associated to different sorption sites. The presence of amine groups and carboxylic groups with their proper acid-base properties and with their proper ability to bind metal ions through chelation and ion-exchange mechanisms offer a wide range of possibilities for sorbent interaction with U(VI). Amino groups may bind uranyl ions through chelation and the competition of protons in acid solutions (amine protonation) limits U(VI) binding. Counter anions of the acid used for pH control enter in competition with uranyl species for metal binding. The pH increase improves metal sorption. In addition, increasing the pH favors the formation of polynuclear hydrolyzed uranyl species such as $UO_2(OH)^+$, $(UO_2)_2(OH)_2{}^{2+}$, $(UO_2)_3(OH)_5{}^{3+}$, which were reported to be favorable for uranyl sorption on fungal biomass (12). Hydrolysis reactions were described by the following equations (41):

$$UO_2{}^{2+} + 2H_2O \leftrightarrow UO_2(OH)^{+1} + H_3O^+ \qquad pK_1 = 5.8 \tag{5a}$$

$$2UO_2{}^{2+} + 4H_2O \leftrightarrow (UO_2)_2(OH)_2{}^{2+} + 2H_3O^+ \qquad pK_2 = 5.62 \tag{5b}$$

$$3UO_2{}^{2+} + 10H_2O \ll (UO_2)_3(OH)_5{}^{+} + 5H_3O^+ \qquad pK_3 = 15.63 \tag{5c}$$

where pK_s are the logarithms of the equilibrium constants.

On the other hand, in acidic solutions the protonation of amino groups allows the binding of metal anions through ion-exchange mechanisms. The control of the pH with sulfuric acid leads to the possible formation of uranyl sulfate anions such as $UO_2.(SO_4)_2{}^{2-}$ and $UO_2.(SO_4)_3{}^{4-}$ (42), which, in turn, can bind to protonated amine groups through anion exchange. Carboxylic groups may also interact with U(VI), though weakly than amino groups; for example, calcium alginate gel beads were used for U(VI) recovery from acid solutions (16). Optimum conditions were found, in this case, close to pH 3.

From these results it appears that U(VI) sorption may proceed through a combination of interactions of $UO_2{}^{2+}$ with protonated amino groups (anionic uranyl sulfate species) and carboxylic groups in acid solutions (pH 2-3) while in near neutral solutions (around pH 5) chelation may predominate on amino groups by chelation involving uranyl species (free or under the form of polynuclear hydrolyzed species). Next, experiments were performed at initial pH 3.6 (with equilibrium pH close to 5).

Uptake Kinetics

The uptake kinetics for U(VI) recovery using cysteine-functionalized chitosan magnetic nano-based particles is shown in Fig. 7 (sorption capacity vs. time). Three sections can be identified:

a. initial steep slope within the first 5 minutes of contact with a sorption that represent about 50% of total sorption,
b. a second stage (5-50 min time range) where the sorption capacity progressively increases (to reach about 97% of total sorption), and
c. a third step where the sorption is much slower and that represents 3% of total sorption.

This last section is probably associated with the progressive and slow swelling of biopolymer layer with limited effect of

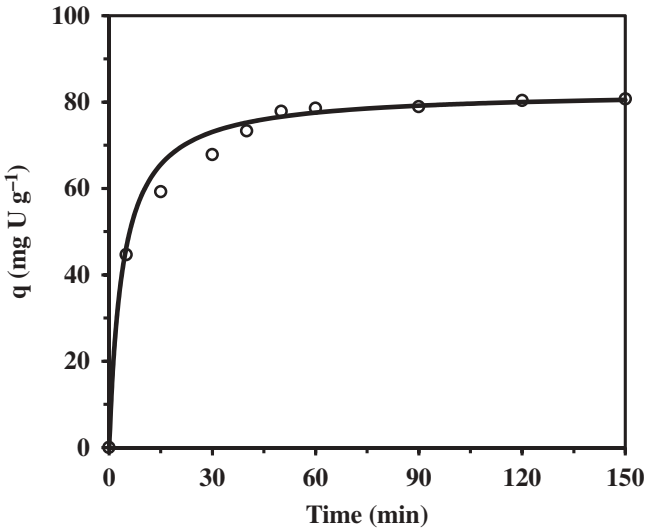

FIG. 7. Uptake kinetics for U(VI) ions sorption using cysteine-functionalized chitosan magnetic nano-based particles (pH_i: 3.6; C_0: 110 mg L^{-1}; T: 25 ± 1°C; SD: 1 g L^{-1}; solid line shows the PSORE model fit of experimental data).

resistance to intraparticle diffusion. The fast sorption (compared with other sorption systems based on chitosan flakes), especially in the initial stage, can be explained by:

(a) the high specific surface area of nano-based sorbent particles, and

(b) the limited effect of resistance to intraparticle diffusion (20, 27).

The second stage is probably controlled by the combination of reaction rate and the swelling effect of cysteine-functionalized chitosan layer. As the sorption sites become progressively covered, the rate of sorption decreased. Basically, 50 min of contact appears to be sufficient for roughly achieving equilibrium.

Actually, most sorption reactions take place through a series of mechanisms such as (43):

i. external film diffusion,
ii. intra-particle diffusion, and
iii. reaction between sorbate and active site (physisorption and/or chemisorption).

The contribution of resistance to film diffusion to kinetic control can be easily reduced by providing a sufficient agitation with an agitation speed of 250 rpm the effect of film diffusion can be neglected. This is confirmed by the steep initial slope of kinetic curve; film diffusion is usually considered the most significant during the first minutes of contact. Uptake kinetics has been modelled using four models: the so-called pseudo-first and pseudo-second order rate equations, the Elovich model, and the simplified model of resistance to intraparticle diffusion (43).

The linear forms of pseudo-first order rate equation (PFORE) and pseudo-second order rate equation (PSORE) are reported in Eqs. (6) and (7), respectively:

$$\log\left(q_{eq} - q(t)\right) = \log q_{eq} - (k_1/2.303)t \quad (6)$$

$$t/q(t) = 1/\left(k_2\, q_{eq}{}^2\right) + \left(1/q_{eq}\right)t \quad (7)$$

where q_{eq} and q(t) (mg U g^{-1}) are the sorption capacities at equilibrium and time t (min), respectively. k_1 (min^{-1}) and k_2 (g mg^{-1} min^{-1}) are the rate constant of pseudo-first-order and the rate constant of pseudo-second-order of adsorption, respectively.

The Elovich model is generally associated to chemisorption and is based on the same assumption as the Temkin isotherm model. It is commonly used for describing the kinetics of chemical sorption of gases, but it is frequently extended to liquid phase sorption:

$$q(t) = A_E + B_E\, Lnt = 1/\beta\ Ln(\alpha\beta) + 1/\beta\ Ln\ t. \quad (8)$$

where A_E (mg g^{-1}) and B_E (mg g^{-1}) are both the Elovich constants; α (mg g^{-1} min^{-1}) is the initial sorption rate and β (g mg^{-1}) is a constant related to the surface coverage and the activation energy for chemical sorption.

TABLE 1
Kinetics parameters and values of R^2 for U(VI) ions sorption

Pseudo first-order rate equation (PFORE)		
K_1 (min^{-1})	q_e, (mg/g)	R^2
5.9 x 10^{-2}	58.3	0.952
Pseudo second-order rate equation (PSORE)		
K_2 (g mg^{-1} min^{-1})	q_e, (mg/g)	R^2
31.1 x 10^{-4}	82.6	0.999
Intraparticle diffusion simplified model (IDSM)		
C (mg g^{-1})	K_p (mg g^{-1} $min^{-0.5}$)	R^2
27.3	5.65	0.726
Elovich equation		
B_E (mg g^{-1})	A_E (mg g^{-1})	R^2
15.7	11.3	0.926

The resistance to intraparticle diffusion can be approached by a simplified equation (IDSM):

$$q(t) = k_{int.}t^{0.5} + c \quad (9)$$

where $k_{int.}$ (mg g^{-1} $min^{-0.5}$) is the intraparticle diffusion constant.

The experimental data have been fitted by the aforementioned kinetics models, and their specific parameters (together with their respective correlation coefficients, R^2) are reported in Table 1. Experimental uptake kinetics was plotted after linearization using the different models (See Additional Material Section, Fig. AM1). The PSORE clearly fits better experimental data than the other models (including PFORE, Figure AM1a) as shown in both Table 1 and Fig. AM1b (see Additional Material Section). The plot of q(t) vs. square root of time shows non-linear distribution of modelled points (Fig. AM1c, See Additional Material Section). This is another confirmation that the resistance to intraparticle diffusion is not playing a key role in the control of uptake kinetics. The nano-size of sorbent particles and the thin layer of active polymer at the surface of magnetic cores can easily explain this conclusion.

These results mean that the uptake kinetics is controlled by the rate of chemical sorption that involves valence forces through the sharing or exchange of electrons (complexation, coordination, chelation between reactive groups on modified chitosan, and uranyl species) with negligible effect of mass transfer resistance.

Sorption Isotherms

Figure 8 shows U(VI) sorption isotherm at pH 3.6 (initial pH shifted to 5 ± 0.2 after metal sorption) using cysteine-functionalized chitosan magnetic nano-based particles. The sorption isotherm is characterized by a steep initial slope; the sorption capacity reaches a sorption capacity close to 67 mg U

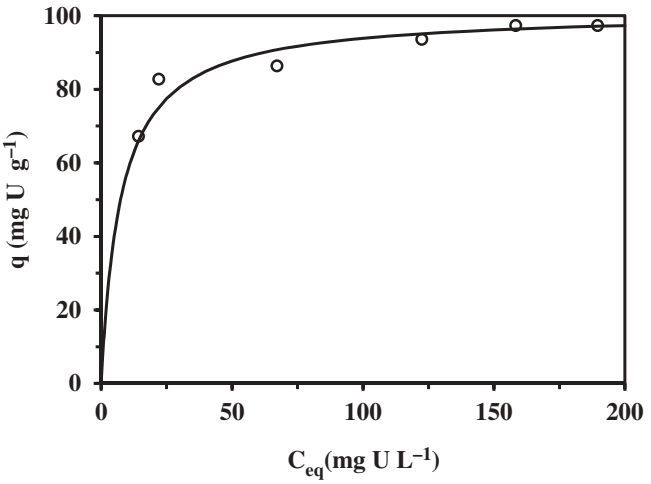

FIG. 8. U(VI) sorption isotherm using cysteine-functionalized chitosan magnetic nano-based particles (pH_i: 3.6; time: 50 min; T: 25 ± 1 °C; SD: 1 g L^{-1}; solid line shows the Langmuir model fit of experimental data).

g^{-1} (i.e., about 70% of the maximum sorption capacity) for a residual metal concentration of 14 mg U L^{-1}. The sorption capacity then progressively increases with increasing metal concentration up to 97.5 mg U g^{-1} (or 0.41 mmol U g^{-1}) for a residual concentration close to 200 mg U L^{-1}. Taking into account the content of inactive magnetic core in the sorbent that represent about 50% of total sorbent mass the sorption capacity tends to 200 mg U g^{-1} (cysteine-functionalized mass), or 0.83 mmol U g^{-1}(biopolymer).

The sorption equilibrium data have been analyzed using different equations, such as Langmuir, Freundlich, and Dubinin–Radushkevich (D–R) isotherm models (44). The asymptotic shape of the sorption isotherm (Fig. 8) suggests that the Langmuir equation is probably more appropriate for fitting experimental data than the other equations (e.g., the exponential trend of the Freundlich equation is not consistent with the profile of the curve).

The Langmuir model is based on the assumption that sorption sites are identical and energetically equivalent, and that sorption occurs at monolayer coverage (44, 45). The equilibrium relationship is described by Eq. (10a) (and its linearized form, Eq. 10b):

$$q = q_m.b.C_{eq}/(1 + b.C_{eq}) \quad (10a)$$

$$C_{eq}/q = (1/q_{max.})C_{eq} + (1/(b.q_{m.})) \quad (10b)$$

where q is the amount of metal ions sorbed at equilibrium (mg U g^{-1}), C_{eq} is the equilibrium metal ion concentration in the aqueous (mg U L^{-1}), q_m is the maximum adsorption capacity of the sorbent (mg U g^{-1}), and b is the Langmuir sorption constant (L mg^{-1}), respectively.

According to the Langmuir model, the experimental data were plotted as C_e/q_e versus C_e (Figure AM2b, See Supplemental material section). The values of Langmuir constants q_m and b were obtained by linear regression method (Table 2). The high value of the correlation coefficient confirms the suitability of the Langmuir equation for describing the distribution at equilibrium of the sorbate between the solution and the sorbent. Providing that physical characterization method could support the hypotheses of the Langmuir model, the sorption process can be assimilated to monolayer sorption onto a surface with finite number of identical sites, which are homogeneously distributed over the sorbent surface. This hypothesis is probably not supported by the presence of different possible sorption sites such as amino groups and carboxylic groups with not necessarily identical sorption energies. On the other hand, the contribution of carboxylic groups at equilibrium pH 5 may be negligible compared to the contribution of amino groups.

TABLE 2
Isotherm constants and values of R^2 for U(VI) ions sorption

Langmuir isotherm constants		
q_m	b (L mg^{-1})	R^2
101.0	0.132	0.999
Freundlich isotherm constants		
n	K_F (mg g^{-1})	R^2
8.16	52.0	0.875
Temkin isotherm constants		
A_T (mg g^{-1})	B_T (mg g^{-1})	R^2
83.7	10.2	0.900
D-R isotherm constants		
$q_{m.}$	E_{ad} (kJ mol^{-1})	R^2
99.3	8.51	0.903

The dimensionless constant, R_L, reflects the favorability of the sorption process using the affinity constant of the Langmuir equation, b, according to Eq. (11) (44).

$$R_L = 1/(1 + bC_o) \quad (11)$$

where C_o is the initial concentration of the U(VI) ions for selected experiment. Regardless of the initial concentration the value of R_L varies in the range 0.035 to 0.026; this means much smaller than 1.0, and that the sorption is very favorable whatever the concentrations range.

The Freundlich isotherm model is based on the assumption of an exponentially decaying sorption site energy distribution (44, 46). It is applied to describe heterogeneous system characterized by a heterogeneity factor of n. The Freundlich model is given by Eq. (12a), and its linearized form, Eq. (12b):

$$q = k_f\ C_{eq}^{\ 1/n} \quad (12a)$$

TABLE 3
Comparison of sorption capacity for UO_2^{2+} ions with various sorbents

Sorbent material	Initial pH	Time (min)	T (°C)	SD (g L^{-1})	C_0 (mg U L^{-1})	q_m (mg U g^{-1})	Isotherm model	Kinetic model	Ref.
Magnetite nanoparticles	7	360	27	1	50	5	————	——-	(50)
Magnetic chitosan	5	40	27	10	500	42	Langmuir	———	(51)
Cross-linked chitosan with epichlorohydrin	3	120	25	10	90	49.05	Langmuir + Freundlich	PSORE	(18)
Amberlite IRA-910 (mono tertiary amine)	1.39	120	25	1	185.6	64.27	Freundlich	PSORE	(52)
Ethylenediamine/ magnetic chitosan	3	30	30	2	200	82.83	Spis	PSORE	(33)
Diethylenetriamine/ magnetic chitosan	3.5	120	25	0.2	80	62.75	Spis	PSORE	(53)
Tetraethylenpentamine/ magnetic chitosan	4	30	25	1	1428.17	397.52	Langmuir	PSORE	(54)
Cysteine/chitosan magnetic nanoparticles	3.61-5	50	25	1	250	97.5	Langmuir + D-R model	PSORE	*This work*
Magnetic Schiff base	6	360	25	1	100	94.3	Langmuir	PSORE	(35)
Salicylideneimine/ hydrothermal carbon	4.3	120	15	0.5	120	261.8	Langmuir + D-R model	PSORE	(8)

$$\ln q = \ln k_f + 1/n \ln C_{eq} \quad (12b)$$

where k_f is the Freundlich isotherm constant, and n (dimensionless) is the heterogeneity factor. The parameters are obtained from the slope (1/n) and the intercept (ln k_f) of the plot of ln q versus ln C_{eq} (Table 2). The value of 1/n gives an indication of the affinity of the sorbent for target solute (and the "favorability" of the sorption process), when $1/n < 1$ the sorption is very favorable on the entire range of concentration, while $1/n > 1$ means that the sorption is favorable only at high solute concentration. In this study, the value of 1/n being less than 1.0 the sorption can be considered as favorable over the entire concentration range.

The Dubinin-Radushkevich isotherm model is usually employed for characterizing the physical or chemical nature of the sorption process. The D-R equation is defined by Eq. (13) (44, 47).

$$\ln q = \ln q_D - K_{DR}\, \varepsilon^2 \quad (13)$$

where q_D is the theoretical saturation capacity, and ε is the Polanyi potential is equal to [$\varepsilon = RT \ln(1 + 1/C_{eq})$]. K_{DR} is related to the mean free sorption energy per molecule of sorbate, R is the universal gas constant (8.314 J $mol^{-1}K^{-1}$) and T is the absolute temperature, K.

The D-R constant (K_{DR}) give valuable information on the mean energy of sorption E_{DR} (kJ/mol), which quantify the free energy exchanged for the transfer of one mole of solute from the infinity (i.e., the solution) and the sorbent surface. E_{DR} provides information about chemical and physical sorption, and can be determined according to $E_{DR} = (-2K_{DR})^{-1/2}$; in the range 1-8 kJ mol^{-1} E_{DR} describes a physical sorption, while chemical sorption corresponds to a mean energy higher than 8 kJ mol^{-1} (44, 47).

The plot of ln q versus ε^2 gives a straight line with a slope (K_{DR}) and an intercept (ln q_D) as shown in Fig. AM2b (See Supplemental Material Section). The parameters are reported in Table 2. The value of the mean sorption energy (E_{DR}) is in the range of 8–16 kJ mol^{-1} indicating that the sorption is predominantly a chemisorption process. Furthermore, this is consistent with the strong interaction between the metal ion and the ligand on sorbent surface.

The Temkin equation was also used to model the sorption isotherm. The Temkin isotherm takes into account the interactions between sorbent particles and metal ions assuming that the free energy of sorption is a function of the surface coverage (44, 48). The isotherm is described by Eq. (14):

$$q = B_T \ln C_{eq} + B_T \ln A_T \quad (14)$$

where A_T is the equilibrium binding constant corresponding to the maximum binding energy, B_T is a constant related to surface heterogeneity of the adsorbent, T is the temperature (K), and R is the ideal gas constant (8.314 J mol^{-1} K^{-1}). Thus the constants can be obtained from the slope and intercept of a straight line plot of q versus ln C_{eq}. The constants of the Temkin model are listed in Table 4. The constant A_T reflects the initial sorption heat of the sorbent: the greater A_T value the

higher the sorption heat and the greater the affinity of the sorbent for the sorbate. This value confirms the strong interaction between U(VI) and the reactive groups at the surface of the sorbent.

Comparison of Sorption Capacity for UO_2^{2+} with other Sorbents

Table 3 compares the maximum sorption capacities of different sorbents for UO_2^{2+} ions. Although these data were obtained under different experimental conditions, they represent a useful criterion for the comparison of sorption performance. This table confirms that the resin exhibit good sorption performance comparable with other chitosan-based materials or synthetic resins; the resin combines both good sorption capacities and fast kinetic characteristics. This may be attributed to the formation of an extended polymeric film of modified chitosan at the surface of magnetic particles; this induces a larger number of exposed active sites for interaction with UO_2^{2+} ions. The grafting of cysteine moiety brings additional functional groups that may:

i. increase the density of sorption site,
ii. change the sorption sites and mechanisms (depending on the pH), which, in turn, increase sorption capacity and selectivity for UO_2^{2+} ions.

In addition, the incorporation of a magnetic core contributes to improving the ready recovery of the particles at the end of the sorption process through an external magnet making easier the management of the system in hazardous operational conditions.

Other sorbents using amidoxime/acrylic acid composites have been recently tested for the sorption of uranium from seawater. Very high sorption capacities were reported under very different experimental conditions: a simulated seawater (containing more than 10 g L^{-1} of Na^+, more than 15 g L^{-1} of Cl^- and up to 140 mg L^{-1} of HCO_3^-) was spiked with uranyl ions (at a concentration close to 6 mg U L^{-1}) at pH 8 (49). At long contact times (42-56 days) sorption capacities up to 161-179 mg U g^{-1} were obtained (with sorption efficiencies close to 55-62%). Even in the presence of carbonate ions (which may influence metal speciation and uranyl availability) the sorption capacity remains very high. This is a very competitive property compared to conventional materials. Uranyl sorption in the presence of carbonate has not been tested with the present sorbent; however, based on the mechanisms supposed to be involved in metal binding, a decrease in sorption properties is expected.

Effect of Temperature on U(VI) Sorption-Thermodynamics

To study the effect of temperature on sorption of UO_2^{2+} ions, experiments were carried in the range 298-323 ± 1°K. Uranyl sorption decreases with increasing the temperature from 175 mg U g^{-1} to 123 mg U g^{-1} (between 298 K and 323 K, 25-50°C). The sorption process is exothermic. The thermodynamic parameters (i.e., Gibbs free energy change, ΔG^o; enthalpy change, ΔH^o; and entropy change, ΔS^o) were obtained and derived from the van't Hoff equation (52):

$$\ln K_d = (-\Delta H^\circ/R)\ 1/T + \Delta S^\circ/R \quad (15)$$

$$\Delta G^\circ = \Delta H^\circ - T\Delta S^\circ \quad (16)$$

where K_d is the distribution coefficient, R is the universal gas constant (8.314 J mol^{-1} K^{-1}), and T is the absolute temperature (K).

The enthalpy change and the entropy change are deduced from the slope (-ΔH°/R) and the intercept (ΔS°/R) of the linear regression of ln K_d versus 1/T (Fig. 9). The values of ΔH^o (-11.85 kJ mol^{-1}) and ΔS^o (59 J mol^{-1} K^{-1}) are reported together with the Gibbs free energy, ΔG^o in Table 4. The negative value of ΔH^o confirms the exothermic nature of the sorption process; the reaction becomes more favorable at room temperature. The exothermic nature of sorption has also been reported for U(VI) sorption on ethylenediamine-modified magnetic chitosan (33), magnetic Schiff base (35), and ion-imprinted and non-imprinted magnetic chitosan resins (55). The study of U(VI) sorption on

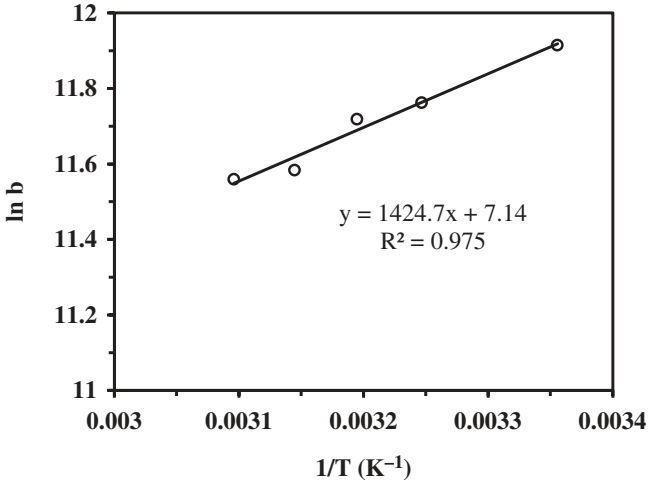

FIG. 9. Van't Hoff plot of ln K_d against 1/T for U(VI) sorption using cysteine-functionalized chitosan magnetic nano-based particles.

TABLE 4
Thermodynamic parameters of U(VI) ions sorption

Temp. (K)	ΔH^o (kJ mol^{-1})	ΔS^o (J mol^{-1} K^{-1})	ΔG^o (kJ mol^{-1})	$T\Delta S^o$, (kJ mol^{-1})	R^2
298	–11.845	59.0	–29.5	17.7	0.975
308			–30.1	18.3	
313			–30.4	18.6	
318			–30.7	18.9	
323			–31.0	19.2	

tetraethylenepentamine/GMA (56), and salicylideneimine–functionalized hydrothermal carbon (8), Amberlite IRA-910 resin (52) showed a different trend; these materials exhibited endothermic sorption. The values of enthalpy are coherent with chemical nature of the interaction, which confirms the formation of a complex between active sites and UO_2^{2+} ions. The negative values of ΔG^o indicate the spontaneous nature of sorption process, and the decrease in the values of ΔG^o with increasing temperature suggests that the sorption process becomes more spontaneous at low temperature (8). At the highest temperatures the interactions between the sorbent and metal ions become weaker, leading to lower sorption capacities (35, 57). Also, the data showed that $|\Delta H°| < |T\Delta S°|$ in the studied temperature range. This indicated that the sorption process was dominated by entropy changes rather than enthalpy changes (52). The positive value of entropy change means that the randomness of the system increased during sorption (increase in the disorder of the system associated to a possible release of water molecules from hydration spheres).

Metal Desorption and Sorbent Recycling

In most cases, the desorption of metal ions loaded on biosorbents is processed by pH change to reverse the binding mechanism. Using concentrated acid (molar solutions of nitric or hydrochloric acid, for example) is thus generally sufficient for eluting sorbed metals from the sorbent matrix, providing the matrix remains stable under selected conditions. In the present case, excessive acidity may cause the chemical degradation (dissolving) of the magnetic core of sorbent particles (i.e., Fe_3O_4). Generally, the sorbed metal ions can be desorbed and concentrated by eluant. It is preferable using a chelating agent, such as ethylenediamine tetraacetic acid (EDTA), thiourea, and urea, which are very efficient for metal complexation in a broad range of pH. A solution of urea (0.5 M) acidified with a few drops of H_2SO_4 (0.2 M) was chosen as the eluant for uranyl. The recycling was repeated for five successive cycles and the results are shown in Table 5. Though the sorption capacity and efficiency progressively decrease with the number of operating cycles, even after five cycles the sorption performance remains very high, the sorption efficiency decreases from 100% to little less than 92% while the sorption capacity decreases by less than 9% in the fifth cycle.

TABLE 5
Sorption cycles of the adsorbent

Cycle	q_e (mg g^{-1})	Adsorption efficiency (%)
Cycle I	97.3	100.0
Cycle II	91.9	94.4
Cycle III	90.6	93.1
Cycle IV	89.6	92.1
Cycle V	89.2	91.6

CONCLUSIONS

Cysteine-functionalized chitosan magnetic nano-based particles has been successfully synthesized, characterized and tested for uranium sorption from synthetic acid solutions (pH being controlled with sulfuric acid). Despite a small aggregation (40-50 nm) of nanoparticles (about 13.5 nm in size) under the effect of dipole-dipole attraction, the sorbent maintains a sub-micronic size. The magnetic properties have been quantified and have been used for solid-liquid separation.

The maximum sorption capacities were found to be 97 mg g^{-1} for uranium ions at pH 3.6. Temperature shows a negative effect on UO_2^{2+} ions sorption. The reaction is exothermic (ΔH= -11.85 kJ/mol), spontaneous, and leads to an increased randomness. The Langmuir equation fits well the sorption isotherms while the uptake kinetics are controlled by the pseudo-second order rate equation. The nano-size of sorbent particles and the thin layer of active biopolymer at the surface of magnetic core particles make negligible the impact of resistance to intraparticle diffusion. Finally, the sorbent can be regenerated with high efficiency using acidified urea (0.5 mol L^{-1}) as the eluent; and the sorbent can be recycled for at least 5 sorption/desorption cycles.

ACKNOWLEDGEMENTS

Special dedication to the memory of Prof. Ahmed Donia.

FUNDING

This work was supported by the French government through a fellowship (A.A. Glahoum) granted by the French Embassy in Egypt (Institut Français d'Egypte).

SUPPLEMENTAL MATERIAL

Supplemental data for this article can be accessed on the publisher's website.

REFERENCES

1. Li, B.; Raff, J.; Barkleit, A.; Bernhard, G.; Foerstendorf, H. (2010) Complexation of U(VI) with highly phosphorylated protein, phosvitin A vibrational spectroscopic approach. *J. Inorg. Biochem. 104*(7): 718–725.
2. Zhang, X.-F.; Ding, C.-L.; Liu, H.; Liu, L.-H.; Zhao, C.-Q. (2011) Protective effects of ion-imprinted chitooligosaccharides as uranium-specific chelating agents against the cytotoxicity of depleted uranium in human kidney cells. *Toxicology 286*(1–3): 75–84.
3. Liao, X. P.; Lu, Z. B.; Du, X.; Liu, X.; Shi, B. (2004) Collagen fiber immobilized *Myrica rubra* tannin and its adsorption to UO_2^{2+}. *Environ. Sci. Technol. 38*(1): 324–328.
4. Mellah, A.; Chegrouche, S.; Barkat, M. (2006) The removal of uranium (VI) from aqueous solutions onto activated carbon: Kinetic and thermodynamic investigations. *J. Colloid Interface Sci. 296*(2): 434–441.

5. Roosen, J.; Binnemans, K. (2014) Adsorption and chromatographic separation of rare earths with EDTA- and DTPA-functionalized chitosan biopolymers. *J. Mater. Chem. A 2*(5): 1530–1540.
6. Roig, M. G.; Manzano, T.; Diaz, M. (1997) Biochemical process for the removal of uranium from acid mine drainages. *Water Res*. *31*(8): 2073–2083.
7. Kim, J.; Tsouris, C.; Mayes, R. T.; Oyola, Y.; Saito, T.; Janke, C. J.; Dai, S.; Schneider, E.; Sachde, D. (2013) Recovery of uranium from seawater: A review of current status and future research needs. *Sep. Sci. Technol*. *48* (3): 367–387.
8. Wang, H.; Ma, L.; Cao, K.; Geng, J.; Liu, J.; Song, Q.; Yang, X.; Li, S. (2012) Selective solid-phase extraction of uranium by salicylideneimine-functionalized hydrothermal carbon. *J. Hazard. Mater. 229*: 321–330.
9. Cao, Q.; Liu, Y.; Kong, X.; Zhou, L.; Guo, H. (2013) Synthesis of phosphorus-modified poly(styrene-co-divinylbenzene) chelating resin and its adsorption properties of uranium(VI). *J. Radioanal. Nucl. Chem*. *298*(2): 1137–1147.
10. Volesky, B. (2003) Biosorption process simulation tools. *Hydrometallurgy 71*(1–2): 179–190.
11. Naja, G.; Mustin, C.; Volesky, B.; Berthelin, J. (2008) Biosorption study in a mining wastewater reservoir. *Int. J. Environ. Pollut*. *34*(1–4): 14–27.
12. Guibal, E.; Roulph, C.; Lecloirec, P. (1992) Uranium biosorption by a filamentous fungus *Mucor miehei*: pH effect on mechanisms and performances of uptake. *Water Res*. *26*(8): 1139–1145.
13. Vogel, M.; Guenther, A.; Rossberg, A.; Li, B.; Bernhard, G.; Raff, J. (2010) Biosorption of U(VI) by the green algae *Chlorella vulgaris* in dependence of pH value and cell activity .*Sci. Total Environ*. *409*(2): 384–395.
14. Kausar, A.; Bhatti, H. N.; MacKinnon, G. (2013) Equilibrium, kinetic and thermodynamic studies on the removal of U(VI) by low cost agricultural waste. *Colloids Surf*., *B 111*: 124–133.
15. Prodromou, M.; Pashalidis, I. (2013) Uranium adsorption by non-treated and chemically modified cactus fibres in aqueous solutions. *J. Radioanal. Nucl. Chem*. *298*(3): 1587–1595.
16. Bai, J.; Fan, F.; Wu, X.; Tian, W.; Zhao, L.; Yin, X.; Fan, F.; Li, Z.; Tian, L.; Wang, Y. (2013) Equilibrium, kinetic and thermodynamic studies of uranium biosorption by calcium alginate beads. *J. Environ. Radioactiv. 126*: 226–231.
17. Guibal, E.; Jansson Charrier, M.; Saucedo, I.; Lecloirec, P. (1995) Enhancement of metal-ion sorption performances of chitosan: Effect of the structure on the diffusion properties. *Langmuir 11*(2): 591–598.
18. Wang, G. H.; Liu, J. S.; Wang, X. G.; Xie, Z. Y.; Deng, N. S. (2009) Adsorption of uranium (VI) from aqueous solution onto cross-linked chitosan. *J. Hazard. Mater. 168*(2–3): 1053–1058.
19. Guibal, E. (2004) Interactions of metal ions with chitosan-based sorbents: A review. *Sep. Purif. Technol*. *38*(1): 43–74.
20. Shukla, S. K.; Mishra, A. K.; Arotiba, O. A.; Mamba, B. B. (2013) Chitosan-based nanomaterials: A state-of-the-art review. *Int. J. Biol. Macromol*. *59*: 46–58.
21. Gao, Y. H.; Oshita, K.; Lee, K. H.; Oshima, M.; Motomizu, S. (2002) Development of column-pretreatment chelating resins for matrix elimination/multi-element determination by inductively coupled plasma-mass spectrometry. *Analyst 127*(12): 1713–1719.
22. Donia, A. M.; Atia, A. A.; Daher, A. M.; Desouky, O. A.; Elshehy, E. A. (2011) Synthesis of amine/thiol magnetic resin and study of its interaction with Zr(IV) and Hf(IV) ions in their aqueous solutions. *J. Dispersion Sci. Technol*. *32*(5): 634–641.
23. Filha, V.; Wanderley, A. F.; de Sousa, K. S.; Espinola, J. G. P.; da Fonseca, M. G.; Arakaki, T.; Arakaki, L. N. H. (2006) Thermodynamic properties of divalent cations complexed by ethylenesulfide immobilized on silica gel. *Colloids Surf., A 279* (1–3): 64–68.
24. Oshita, K.; Sabarudin, A.; Takayanagi, T.; Oshima, M.; Motomizu, S. (2009) Adsorption behavior of uranium(VI) and other ionic species on cross-linked chitosan resins modified with chelating moieties. *Talanta 79* (4): 1031–1035.
25. Oshita, K.; Takayanagi, T.; Oshima, M.; Motomizu, S. (2007) Adsorption behavior of cationic and anionic species on chitosan resins possessing amino acid moieties. *Anal. Sci*. *23*(12): 1431–1434.
26. Guibal, E.; Vincent, T.; Navarro, R. (2014) Metal ion biosorption on chitosan for the synthesis of advanced materials. *J. Mater. Sci*. *49*(16): 5505–5518.
27. Xue, X.; Wang, J.; Mei, L.; Wang, Z.; Qi, K.; Yang, B. (2013) Recognition and enrichment specificity of Fe_3O_4 magnetic nanoparticles surface modified by chitosan and *Staphylococcus aureus* enterotoxins A antiserum. *Colloids Surf*., *B 103*: 107–113.
28. Marczenko, Z. (1976) *Spectrophotometric Determination of Elements;* Ellis Horwood Series in Analytical Chemistry; Ellis Horwood: Chichester, U. K.
29. Namdeo, M.; Bajpai, S. K. (2008) Chitosan-magnetite nanocomposites (CMNs) as magnetic carrier particles for removal of Fe(III) from aqueous solutions. *Colloids Surf., A 320* (1–3): 161–168.
30. Wan Ngah, W. S.; Endud, C. S.; Mayanar, R. (2002) Removal of copper (II) ions from aqueous solution onto chitosan and cross-linked chitosan beads. *React. Funct. Polym*. *50*(2): 181–190.
31. Donia, A. M.; Atia, A. A.; Abouzayed, F. I. (2012) Preparation and characterization of nano-magnetic cellulose with fast kinetic properties towards the adsorption of some metal ions. *Chem. Eng. J. 191*: 22–30.
32. Martinez, L.; Agnely, F.; Leclerc, B.; Siepmann, J.; Cotte, M.; Geiger, S.; Couarraze, G. (2007) Cross-linking of chitosan and chitosan/poly(ethylene oxide) beads: A theoretical treatment. *Eur. J. Pharm. Biopharm*. *67* (2): 339–348.
33. Wang, J.-S.; Peng, R.-T.; Yang, J.-H.; Liu, Y.-C.; Hu, X.-J. (2011) Preparation of ethylenediamine-modified magnetic chitosan complex for adsorption of uranyl ions. *Carbohydr. Polym*. *84*(3): 1169–1175.
34. Gonçalves, V. L.; Laranjeira, M. C. M.; Fávere, V. T.; Pedrosa, R. C. (2005) Effect of crosslinking agents on chitosan microspheres in controlled release of diclofenac sodium. *Polim: Cienc. Tecnol*. *15*(1): 6–12.
35. Zhang, X.; Jiao, C.; Wang, J.; Liu, Q.; Li, R.; Yang, P.; Zhang, M. (2012) Removal of uranium(VI) from aqueous solutions by magnetic Schiff base: Kinetic and thermodynamic investigation. *Chem. Eng. J. 198*: 412–419.
36. Hosoba, M.; Oshita, K.; Katarina, R. K.; Takayanagi, T.; Oshima, M.; Motomizu, S. (2009) Synthesis of novel chitosan resin possessing histidine moiety and its application to the determination of trace silver by ICP-AES coupled with triplet automated-pretreatment system. *Anal. Chim. Acta 639*(1–2): 51–56.
37. Coates, J. (2000) Interpretation of Infrared Spectra, A Practical Approach. In *Encyclopedia of Analytical Chemistry*; Meyers, R. A., Ed.; Wiley: Chichester, U.K., pp. 10815–10837.
38. Zhou, L.; Xu, J.; Liang, X.; Liu, Z. (2010) Adsorption of platinum(IV) and palladium(II) from aqueous solution by magnetic cross-linking chitosan nanoparticles modified with ethylenediamine. *J. Hazard. Mater. 182* (1–3): 518–524.
39. Guinier, A.; Lorrain, P.; Sainte-Marie Lorrain, D. (1963) *X-ray Diffraction in Crystals, Imperfect Crystals, and Amorphous Bodies*; W.H. Freeman & Co: San Francisco, CA.
40. Kyzas, G. Z.; Deliyanni, E. A. (2013) Mercury(II) removal with modified magnetic chitosan adsorbents. *Molecules 18*(6): 6193–6214.
41. Baes, C. F., Jr.; Mesmer, R. E. (1976) *Hydrolysis of Cations;* Wiley: NY.
42. Ritcey, G. M.; Ashbrook, A. W. (1984) *Solvent Extraction: Principles and Applications to Process Metallurgy;* Elsevier: Amsterdam; Vol. 1.
43. Qiu, H.; Lv, L.; Pan, B.; Zhang, Q.; Zhang, W.; Zhang, Q. (2009) A critical review in adsorption kinetic models. *J. Zhejiang Univ. Sci. A*, *10*: 716–724.
44. Foo, K. Y.; Hameed, B. H. (2010) Insights into the modeling of adsorption isotherm systems. *Chem. Eng. J. 156*(1): 2–10.
45. Langmuir, I. (1918) The adsorption of gases on plane surfaces of glass, mica and platinum. *J. Amer. Chem. Soc. 40*: 1361–1402.
46. Freundlich, H. M. F. (1906) Uber die adsorption in lasungen. *Z. Phys. Chem*. *57*: 385–470.
47. Dubinin, M. M.; Zaverina, E. D.; Radushkevich, L. V. (1947) Sorption and structure of active carbons. I. Adsorption of organic vapors. *Zh. Fiz. Khim*. *21*: 1351–1362.
48. Temkin, V. P. (1940) Kinetics of ammonia synthesis on promoted iron catalysts. *Acta Physiochim*. *12*: 217–222.
49. Saito, T.; Brown, S.; Chatterjee, S.; Kim, J.; Tsouris, C.; Mayes, R. T.; Kuo, L.-J.; Gill, G.; Oyola, Y.; Janke, C. J. (2014) Uranium recovery

from seawater: development of fiber adsorbents prepared via atom-transfer radical polymerization. *J. Mater. Chem. A 2*(35): 14674–14681.
50. Das, D.; Sureshkumar, M. K.; Koley, S.; Mithal, N.; Pillai, C. G. S. (2010) Sorption of uranium on magnetite nanoparticles. *J. Radioanal. Nucl. Chem. 285*(3): 447–454.
51. Stopa, L. C. B.; Yamaura, M. (2010) Uranium removal by chitosan impregnated with magnetite nanoparticles: adsorption and desorption. *Int. J. Nucl. Energy Sci. Technol. 5*(4): 283–289.
52. Rahmati, A.; Ghaemi, A.; Samadfam, M. (2012) Kinetic and thermodynamic studies of uranium(VI) adsorption using Amberlite IRA-910 resin. *Ann. Nucl. Energy 39*(1): 42–48.
53. Xu, J.; Chen, M.; Zhang, C.; Yi, Z. (2013) Adsorption of uranium(VI) from aqueous solution by diethylenetriamine-functionalized magnetic chitosan. *J. Radioanal. Nucl. Chem. 298*(2): 1375–1383.
54. Elwakeel, K. Z.; Atia, A. A.; Guibal, E. (2014) Fast removal of uranium from aqueous solutions using tetraethylenepentamine modified magnetic chitosan resin. *Bioresour. Technol. 160*, 107–114.
55. Zhou, L.; Shang, C.; Liu, Z.; Huang, G.; Adesina, A. A. (2012) Selective adsorption of uranium(VI) from aqueous solutions using the ion-imprinted magnetic chitosan resins. *J. Colloid Interface Sci. 366*(1): 165–172.
56. Donia, A. M.; Atia, A. A.; Moussa, E. M. M.; El-Sherif, A. M.; El-Magied, M. O. A. (2009) Removal of uranium(VI) from aqueous solutions using glycidyl methacrylate chelating resins. *Hydrometallurgy 95* (3–4): 183–189.
57. Reddy, D. H. K.; Lee, S.-M. (2013) Application of magnetic chitosan composites for the removal of toxic metal and dyes from aqueous solutions. *Adv. Colloid Interface Sci. 201–202*(0): 68–93.